18TH WORLD CONFERENCE ON EARTHQUAKE ENGINEERING
WCEE2024
MILAN

MILAN, ITALY
30TH JUNE - 5TH JULY 2024
www.wcee2024.it

CHALLENGES IN DEVELOPING VERTICAL HAZARD FOR SEISMIC ANALYSIS OF CONCRETE DAMS

N. Simon Kwong[1], Sanaz Rezaeian[2], Andrew J. Makdisi[3], & Nicolas Luco[4]

[1] U.S. Geological Survey, Golden, CO, USA, nkwong@usgs.gov

[2] U.S. Geological Survey, Golden, CO, USA, srezaeian@usgs.gov

[3] U.S. Geological Survey, Golden, CO, USA, amakdisi@usgs.gov

[4] U.S. Geological Survey, Golden, CO, USA, nluco@usgs.gov

Abstract: *The seismic response of concrete dams depends on both the horizontal (H) and vertical (V) components of ground motion (GM), and excluding the V components when conducting response history analyses (RHAs) may underestimate the seismic fragility. Although V components of GM time series could be selected to be consistent with the hazard, hazard curves for the V component (or for short, V hazard curves) are rarely available for evaluating such hazard consistency. One of the challenges in developing V hazard curves in the U.S. Geological Survey (USGS) National Seismic Hazard Model (NSHM) is the lack of ground motion models (GMMs) that directly estimate intensity measures (IMs) for the V component of GM. In this study, we compare alternative approaches of developing V hazard curves. Using a case study in California, we compare V hazard curves computed from GMMs for the V component of GM against those from applying GMMs for the V/H ratios and those from selecting multicomponent time series that are consistent with the H hazard. We discuss and invite feedback on issues such as availability of GMMs, applicability of GMMs, and choice of inputs for ground motion selection and modification (GMSM).*

1. Introduction

Nonlinear response history analysis (RHA), or nonlinear time-history dynamic analysis, is one of the most sophisticated methods that is used for seismic analysis of complex concrete dams (Chopra, 2020; U.S. Army Corps of Engineers, 2016). Concrete dams can be complex not only because of the potential failure modes and consequences from seismic-induced failure such as inundation and loss of life, but also because of the difficulties involved when developing a finite element model (FEM). For example, the FEM should capture nonlinearities in geometry and material arising from the dam, surrounding foundation rock, and impounded water (Federal Emergency Management Agency (FEMA), 2005). Examples of other complexities include dam-water-foundation interaction, modelling boundary conditions, or addressing radiation damping (e.g., Basu and Chopra, 2004; Løkke and Chopra, 2019).

Consistency should be maintained between different levels of analysis; for example, it is unreasonable to use “an assumed earthquake loading” for a highly refined structural analysis (page 19 in FEMA, 2005). Therefore, the degree of sophistication in developing ground motion (GM) time series, or accelerograms, as inputs to nonlinear RHA should be commensurate with the degree of sophistication in developing an FEM. Results from nonlinear RHA of a complex FEM are more sensitive to peculiarities of the input GM time series such as the vertical (V) components of GM than those from nonlinear RHA of a simpler FEM. For instance, while the V components of GM are often ignored in nonlinear RHA of buildings (e.g., Zimmerman et al., 2017), ignoring the V components for dams can substantially underestimate its seismic fragility (e.g., Hariri-Ardebili and

Saouma, 2016). V hazard is also important for concrete dams because inaccuracies on V/horizontal (H) issues matter more for short spectral periods than for long spectral periods (Bozorgnia and Campbell, 2004) and concrete dams usually have short fundamental periods. At the same time, developments in the research topic of ground motion selection and modification (GMSM) for dams have not progressed as much as those for buildings. For example, while seismic design guidelines for buildings consider Conditional Mean Spectra (CMS), those for dams do not (ASCE Structural Engineering Institute, 2017; U.S. Army Corps of Engineers, 2016).

Ideally, both the H and V components of selected multicomponent GM time series should be "consistent" with the seismic hazard at the location of the dam (e.g., Heppermann and Luco, 2020; Lin et al., 2013b). "Consistent" refers to agreement between (1) hazard curves derived from selected GM time series and (2) hazard curves determined from ground motion models (GMMs). However, hazard curves for the V component of GM, or V hazard curves for brevity, are rarely available for evaluating such hazard consistencies or lack thereof. For instance, one of the challenges in developing V hazard curves in the U.S. Geological Survey (USGS) National Seismic Hazard Model (NSHM) is the lack of GMMs that directly estimate intensity measures (IMs) for the V component of GM in subduction zones and stable continental regions (Rezaeian et al., in press).

In this paper, we explore alternatives of varying degrees of simplicity for developing V hazard curves. Using a specific case study in which GMMs for the V component are available, we compare V hazard curves computed from GMMs that directly compute the V component of GM, against those from applying GMMs for V/H ratios to H component GMMs, and those from selecting multicomponent GM time series that are consistent with the H hazard. Before summarizing implications from such comparisons, we first describe the specific case study.

2. Case study

NGA-West2 GMMs for the V component of GM are available for active crustal regimes such as California (Bozorgnia et al., 2014; Bozorgnia and Campbell, 2016a; Gülerce et al., 2017; Stewart et al., 2016). To minimize differences in hazard arising from epistemic uncertainty, we present results for the following GMMs: (1) GMM for the H component of GM by Campbell and Bozorgnia (2014; CB2014), (2) GMM for the V component of GM by Bozorgnia and Campbell (2016a; BC2016V), (3) GMM for V/H ratios by Bozorgnia and Campbell (2016b; BC2016V/H), and (4) correlation model between H and V components of GM by Bozorgnia and Campbell (2016b; BC2016corr). Because these GMMs have already been implemented in MATLAB and are publicly available on GitHub (Kwong et al., 2020; Kwong and Chopra, 2020), we perform probabilistic seismic hazard analysis (PSHA) by combining these GMMs with the Uniform California Earthquake Rupture Forecast, Version 3 (UCERF3) earthquake rupture forecast (ERF) from OpenSHA (Field et al., 2003). We include background seismicity and assume vertical strike-slip faulting for all ruptures in the ERF to focus on hazard differences arising from GMMs rather than those arising from seismic source characterization.

We explore results for San Francisco, California (37.75, -122.4), which is one of several National Earthquake Hazards Reduction Program (NEHRP) test sites. Although V/H ratios are largest for sites on soft soils (Bozorgnia and Campbell, 2004; BSSC, 2009), concrete dams are typically constructed on rock, and dam managers typically perform their own site-specific analyses. Therefore, we present results for $V_{S30} = 760$ m/sec (time-averaged shear-wave velocity in the upper 30 m of subsurface conditions), $Z_{1.0} = 0.1$ km (depth to 1.0 km/sec shear-wave velocity), and $Z_{2.5} = 0.6068$ km (depth to 2.5 km/sec shear-wave velocity), which is the default value in BC2016V. To illustrate the concept of hazard consistency, we select multicomponent GM time series using the Conditional Spectra (CS) approach (Bernier et al., 2016; Jayaram et al., 2011; Kwong et al., 2020). We specify the conditioning period, T^*, to be equal to the fundamental period of a hypothetical dam-water-foundation system, T_1. Although T_1 may not be known precisely in practice (e.g., different phases of dam project), we assume $T_1 = 0.2$ sec for illustration purposes.

3. Uses of vertical hazard curves

V hazard curves are used in two primary contexts for design and evaluation of concrete dams. The first is in the selection of multicomponent GM time series for a building code type of evaluation (Chopra, 2020; FEMA, 2005; U.S. Army Corps of Engineers, 2016). The second context is in the selection of multicomponent GM time series for directly assessing seismic risk (Bernier et al., 2016; Hariri-Ardebili, 2018; Heppermann and Luco, 2020). In general, the former can be considered as an "intensity-based assessment," whereas the latter

as a “risk-based assessment” (Applied Technology Council (ATC), 2012; Lin et al., 2013c; NEHRP Consultants Joint Venture, 2011).

3.1. Ground motion selection for intensity-based assessments

Figure 1 illustrates selection and scaling of recorded GM time series based on the FEMA P-65 federal guidelines for a building code type of evaluation (FEMA, 2005). The first step is to determine a design or target spectrum for the H component of GM. In Figure 1a, this design spectrum is illustrated using the Uniform Hazard Spectrum (UHS) with a return period of 1000 years. This return period corresponds roughly to a 10% probability of exceedance in 100 years, which is one way to define the maximum design earthquake (MDE) (U.S. Army Corps of Engineers, 2016); other choices of return periods for the MDE are possible (e.g., 3000 or 10000 years), depending on the criticality of the dam (Chopra, 2020). Another common choice of return period for hazard is 144 years (or a 50% probability of exceedance in 100 years), which corresponds roughly to the operating basis earthquake (OBE). Given the target spectrum, the second step is to conduct disaggregation of the hazard at the MDE to yield a design earthquake rupture scenario (Bazzurro and Cornell, 1999). The hazard at T_1 in Figure 1a is disaggregated for the H component of GM. Given the design earthquake, the third step is to filter the initial GM database so that the resulting candidate accelerograms have seismological parameters (e.g., tectonic regime, magnitude, source-to-site distance) that are representative of those from the earthquake scenario. Finally, at least three accelerograms are selected and scaled so that their resulting response spectra agree closely to the target spectrum within the bandwidth of interest, which is illustrated in Figure 1 using $0.2T_1$ and $1.5T_1$ to capture higher-mode effects and period lengthening from inelasticity, respectively. Figure 1a demonstrates that the response spectra from the suite of three selected GM time series agree with the design spectrum within the period range of interest. Finally, FEMA P-65 cautions against overly scaling GMs because “when the same simple scaling factors are applied to the other horizontal components and the vertical components for the records selected, the spectral fit is usually not as good for the other components” (page 16 in FEMA, 2005). Therefore, to assess spectral fit for the V component, V hazard is required (e.g., using V hazard curves to derive the UHS for the V component of GM, which is shown by dashed line in Figure 1b to emphasize that V hazard curves are rarely available).

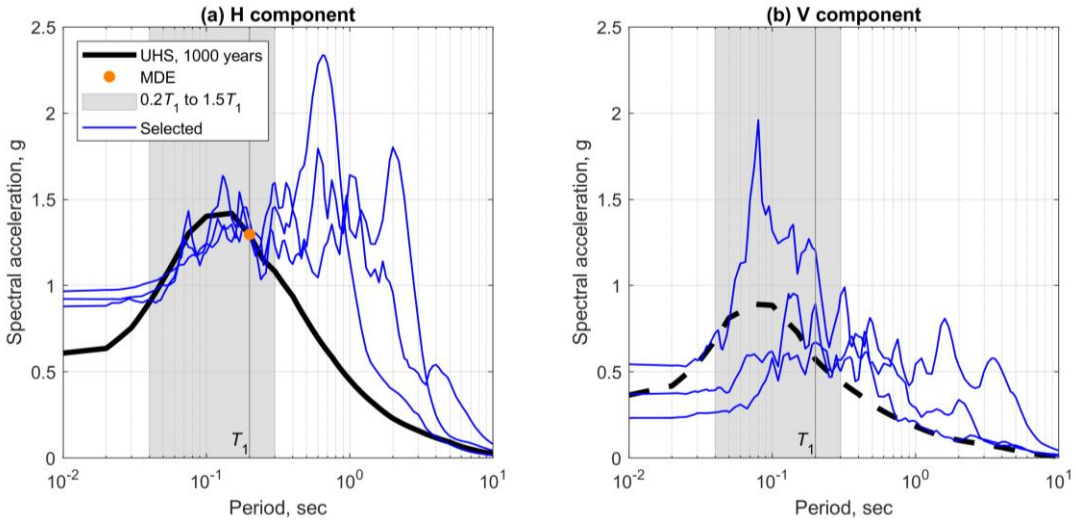

Figure 1. Illustrative example of selecting and scaling recorded ground motion (GM) time series for response history analyses (RHAs) of dams within the context of seismic design and evaluation via FEMA P-65 (FEMA, 2005): (a) horizontal (H) and (b) vertical (V) components of GM. UHS: uniform hazard spectrum; MDE: maximum design earthquake; T_1: fundamental period of dam.

3.2. Ground motion selection for risk-based assessments

Figure 2 illustrates selection and scaling of recorded GM time series for the context of conducting a risk-based assessment (Jalayer, 2003; NEHRP Consultants Joint Venture, 2011). The first step is to choose a conditioning vibration period, T^*. Next, the hazard curve for spectral acceleration at T^* is discretized; in Figure 2a, $T^* = T_1 = 0.2$ sec and the 15 return periods used include the following: 1, 2, 5, 10, 25, 50, 100, 250, 500, 1000, 2500, 5000, 10000, 25000, and 100000 years. At each return period, a set of accelerograms is selected

and scaled to agree with the corresponding CS for the H component of GM at T^*; in Figure 2, a set of 40 multicomponent GM time series was selected and scaled for each of the 15 return periods, leading to a total of 600 multicomponent GM time series. Unlike GMSM as illustrated in Figure 1, GMSM as illustrated in Figure 2 enables direct assessment of risk that is theoretically independent of the choice of T^* and the choice of return period for hazard; however, risk-based assessments involve much more work and depend on hazard consistency of the selected GMs with respect to the hazard curves (e.g., Bradley, 2012; Kwong et al., 2015; Lin et al., 2013b). Therefore, V hazard curves are also used to evaluate hazard consistency of selected GMs before pursuing computationally intensive RHAs.

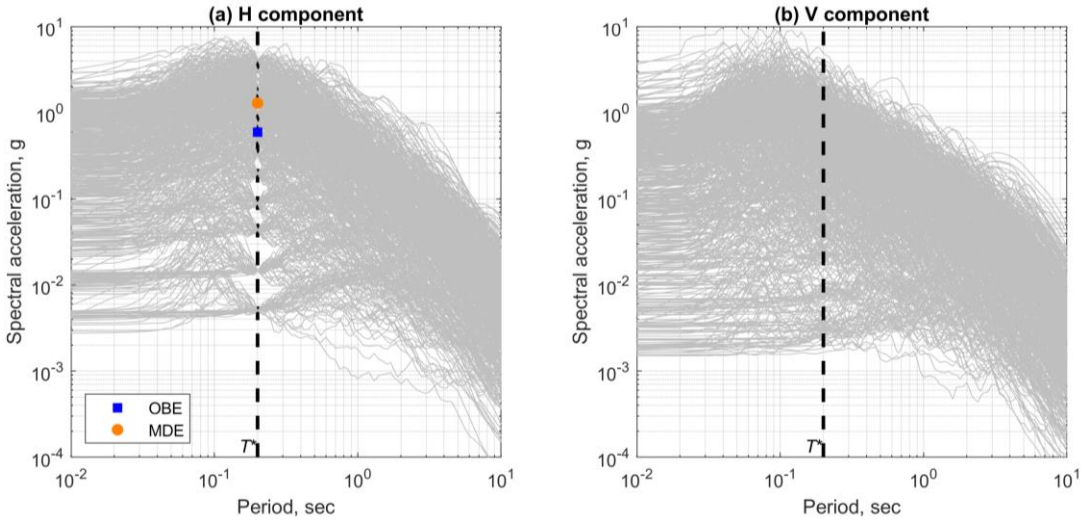

Figure 2. Illustrative example of selecting and scaling multiple sets of recorded GM time series for RHAs of dams within the context of risk-based assessments via NIST GCR 11-917-15 (NEHRP Consultants Joint Venture, 2011): (a) H and (b) V components of GM; vertical dashed lines correspond to the conditioning period. MDE: maximum design earthquake; OBE: operating basis earthquake.

4. Alternative approaches for developing vertical hazard curves

4.1. Direct approach

We consider three approaches for developing V hazard curves. In the first approach, denoted as "direct," we replace the GMM for the H component of GM in the PSHA with the GMM for the V component of GM. More precisely, the hazard curve for spectral acceleration at a given vibration period (and given damping ratio), $\lambda(SA_V \geq a)$, is computed from the following:

$$\lambda(SA_k \geq x) = \sum_{i=1}^{n_{rup}} \Pr(SA_k \geq x \mid rup_i) \times \lambda(rup_i) \quad (1)$$

where $k =$ H or V, n_{rup}, $\lambda(rup_i)$, and $\Pr(SA_V \geq a \mid rup_i)$ denote, respectively, the number of ruptures in the ERF, the annual rate of occurrence for the *i*th rupture, and the probability of spectral acceleration (*SA*) exceeding the IM level x for the *i*th rupture. The probability distribution for $\Pr(SA_k \geq x \mid rup_i)$ is assumed to be lognormal, with medians and logarithmic standard deviations given by a GMM. Using the GMM for the V component of GM by BC2016V as an example, Figure 3 presents the medians and logarithmic standard deviations as functions of vibration period for an earthquake rupture scenario defined by a magnitude of 7.5 and a source-to-site distance of 10 km. If a GMM for the V component of GM was available for a given tectonic regime, Equation 1 can be used to derive the V hazard curve; however, multiple GMMs are needed for capturing epistemic uncertainty in estimating $\Pr(SA_V \geq x \mid rup_i)$ (Abrahamson, 2006).

4.2. Indirect approach

In the second approach, denoted as "indirect," we derive medians and logarithmic standard deviations for the V component of GM from combining a GMM for the H component of GM and a GMM for the V/H ratio, before applying Equation 1. This approach has the advantage of utilizing GMMs for the H component of GM in a

particular tectonic regime to infer data for the V component of GM. More precisely, GMMs for a given vibration period are usually of the form:

$$\ln(SA_k) = \ln\left(SA_{k,m}\right) + dB_k + dW_k \quad (2)$$

where k = H or V and $SA_{k,m}$ denotes the median spectral acceleration; dB and dW denote, respectively, the between-event and within-event residuals, which have zero means but non-zero standard deviations. The standard deviation of dB is denoted by τ, whereas the standard deviation of dW is denoted by ϕ; the total standard deviation is denoted by $\sigma = \sqrt{\tau^2 + \phi^2}$. Equation 2 has been used to derive GMMs for the V/H ratio even though the V/H ratio is not a component of GM (e.g., Bozorgnia and Campbell, 2016b, 2004; Gülerce and Abrahamson, 2011). Outputs from a GMM for the V/H ratio include the median, $[V/H]_m$, and the logarithmic standard deviation, $\sigma_{V/H}$.

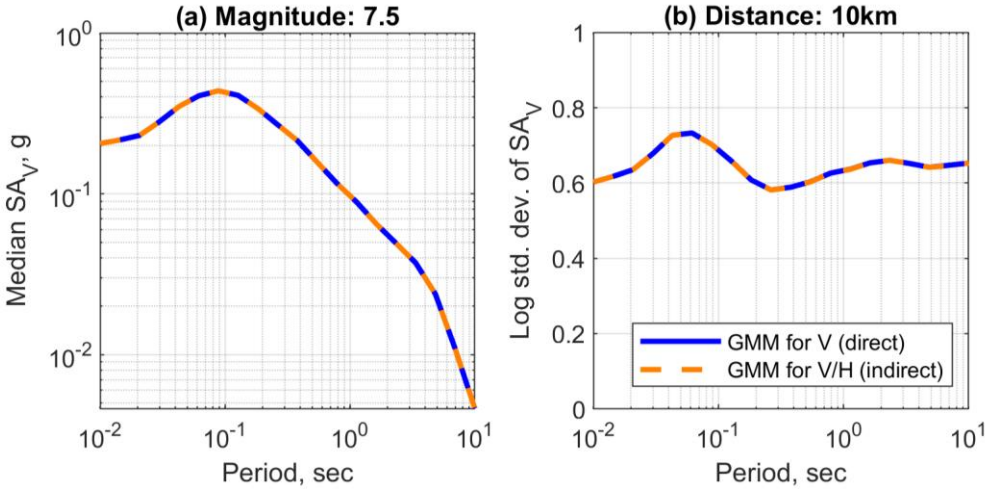

Figure 3. Example comparison of "direct" and "indirect" approaches for deriving ground motion model (GMM) output for vertical (V) and V/horizontal (H) components of ground motion: (a) median and (b) logarithmic standard deviations of vertical spectral acceleration (SA_V).

By definition, the V/H ratio links the H and V components of spectral acceleration at a given vibration period as follows:

$$\ln(SA_V) = \ln(SA_H) + \ln(V/H) \quad (3)$$

Therefore, substituting the random variables in Equation 3 with the functional form from Equation 2 implies that the median for the V component of GM can be derived from (Kwong and Chopra, 2020):

$$SA_{V,m} = SA_{H,m} \times [V/H]_m \quad (4)$$

and the logarithmic standard deviation for the V component of GM can be derived from:

$$\sigma_V = \sqrt{\sigma_H^2 + \sigma_{V/H}^2 + 2\rho_{H,V/H}\sigma_H\sigma_{V/H}} \quad (5)$$

where $\rho_{H,V/H}$ denotes the correlation between the total residual for the H component of GM and the total residual for the V/H ratio. Unlike the GMM for the V/H ratio by Gulerce and Abrahamson 2011 (Gülerce and Abrahamson, 2011), the one by BC2016V/H does not provide estimates of $\rho_{H,V/H}$; instead, the latter provides estimates of (1) the correlation between the between-event residual for the H component of GM and the between-event residual for the V component of GM, $\rho_{H,V}^{(B)}$, and (2) the correlation between the within-event residual for the H component of GM and the within-event residual for the V component of GM, $\rho_{H,V}^{(W)}$. Therefore, we derive a relation herein between $\rho_{H,V/H}$, $\rho_{H,V}^{(B)}$, and $\rho_{H,V}^{(W)}$ as follows:

$$\rho_{H,V/H} = \frac{\rho_{H,V}^{(B)}\tau_H\tau_V + \rho_{H,V}^{(W)}\phi_H\phi_V - \sigma_H^2}{\sigma_H\sigma_{V/H}} \quad (6)$$

Applying Equations 4, 5, and 6 with the case study GMMs leads to the "indirect" medians and logarithmic standard deviations shown in Figure 3, demonstrating internal consistency among the case study GMMs (Bozorgnia and Campbell, 2016a, 2016b; Campbell and Bozorgnia, 2014). Equations 4, 5, and 6 also imply that while epistemic uncertainty in V hazard can be partially captured in the indirect approach by combining multiple GMMs for the H component of GM with a single GMM for the V/H ratio, the epistemic uncertainty can be captured more fully by also considering (i) multiple GMMs for the V/H ratio and (ii) multiple correlation models for estimating $\rho_{H,V/H}$.

4.3. Ground motion selection and modification (GMSM) approach

In the third approach, denoted as "GMSM," we estimate V hazard curves from sets of selected multicomponent GM time series. The GMSM-derived hazard curves are then used to evaluate hazard consistency of a smaller number of GMs before finalizing the selected GMs as inputs to nonlinear RHA. More precisely, the V hazard curve for spectral acceleration at a given vibration period, $\lambda(SA_V(T) \geq y)$, can be expressed analytically as a function of spectral acceleration along the H component of GM at a conditioning vibration period, $SA_H(T^*)$ (e.g., Bradley, 2012; Lin et al., 2013b):

$$\lambda(SA_k(T) \geq y) = \int_x \Pr(SA_k(T) \geq y \mid SA_H(T^*) = x) \times \left|\mathrm{d}\lambda_{SA_H(T^*)}(x)\right| \tag{7}$$

where $k =$ H or V, and $\Pr(SA_k(T) \geq y \mid SA_H(T^*) = x)$ denotes the probability of spectral acceleration exceeding IM level y, conditioned upon the x value of $SA_H(T^*)$. In practice, however, Equation 7 is estimated by discretizing the hazard curve for the conditioning IM, $\lambda_{SA_H(T^*)}(x)$, with a total number of n_{RP} return periods (e.g., 15 return periods):

$$\hat{\lambda}(SA_k(T) \geq y) = \sum_{i=1}^{n_{RP}} \widehat{\Pr}(SA_k(T) \geq y \mid SA_H(T^*) = x_i) \times \left|\mathrm{d}\lambda_{SA_H(T^*)}(x_i)\right| \tag{8}$$

Similarly, Equation 8 can be adapted for exceedance or occurrence of a given limit state (LS) such as concrete cracking instead of spectral acceleration (Hariri-Ardebili and Saouma, 2016). The LS hazard curve can be estimated from :

$$\hat{\lambda}(LS) = \sum_{i=1}^{n_{RP}} \widehat{\Pr}(LS \mid SA_H(T^*) = x_i) \times \left|\mathrm{d}\lambda_{SA_H(T^*)}(x_i)\right| \tag{9}$$

where $\widehat{\Pr}(LS \mid IM^* = x_k)$ denotes the estimated probability of LS exceedance conditioned upon the x_i value of $SA_H(T^*)$.

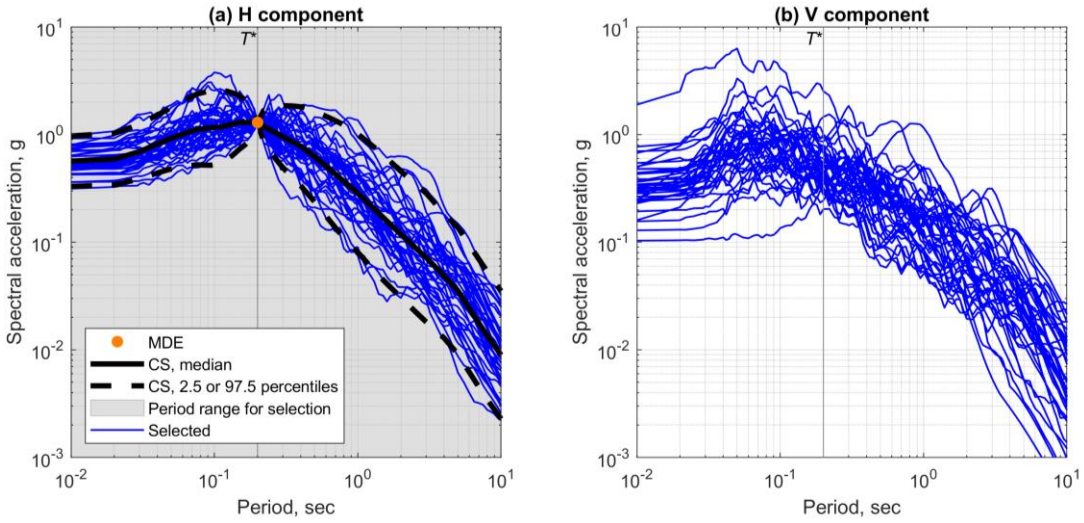

Figure 4. Illustrative example of selecting and scaling one set of recorded ground motion (GM) time series for estimating $Pr(SA_k(T) \geq y \mid SA_H(T^*) = x)$ and $Pr(LS \mid SA_H(T^*) = x)$ via the Conditional Spectrum (CS) approach: (a) horizontal (H) and (b) vertical (V) components of GM. MDE: maximum design earthquake.

The terms $\widehat{\Pr}(SA_k(T) \geq y \mid SA_H(T^*) = x_i)$ and $\widehat{\Pr}(LS \mid SA_H(T^*) = x_i)$ are both estimated from the same set of selected multicomponent GM time series that have been scaled so that $SA_H(T^*) = x_i$. To illustrate this concept, we use the MDE as an example of x_i and use the CS approach as an example of selecting one set of multicomponent GM time series to be consistent with the H hazard (Jayaram et al., 2011). The NGA-West2 GM database was used as a starting point (Ancheta et al., 2014); the sum-of-squares metric was used to quantify spectra comparisons (Jayaram et al., 2011); and scale factors were constrained within a factor of four (NEHRP Consultants Joint Venture, 2011). However, limits on parameters such as magnitude, distance, and site class were not imposed (Tarbali and Bradley, 2016). Figure 4 demonstrates that the selected GM time series agree with the target CS over the period range of 0.01 sec to 10 sec for the H component of GM; however, GM spectra for the V component are allowed to vary uncontrollably. For this intensity level of $SA_H(T^*)$, the fraction of IM exceedances from the selected multicomponent GM time series is used to estimate $\widehat{\Pr}(SA_k(T) \geq y \mid SA_H(T^*) = MDE)$. Repeating the GM selection process for multiple IM levels of $SA_H(T^*)$ leads to results such as those depicted in Figure 2.

5. Comparison of alternative approaches

Figure 5 illustrates evaluation of the sets of selected multicomponent GM time series in terms of hazard consistency along the H component of GM. For spectral acceleration at a given vibration period, the solid blue curve shows the H hazard curve from substituting the CB2014 GMM for the H component of GM into Equation 1 (i.e., "direct" approach). By contrast, the chained black curve shows the H hazard curve from applying Equation 8 to the spectral accelerations along the H component of GM from the $n_{RP} = 15$ sets of multicomponent GMs that condition upon $T^* = T_1 = 0.2$ sec (i.e., "GMSM" approach).

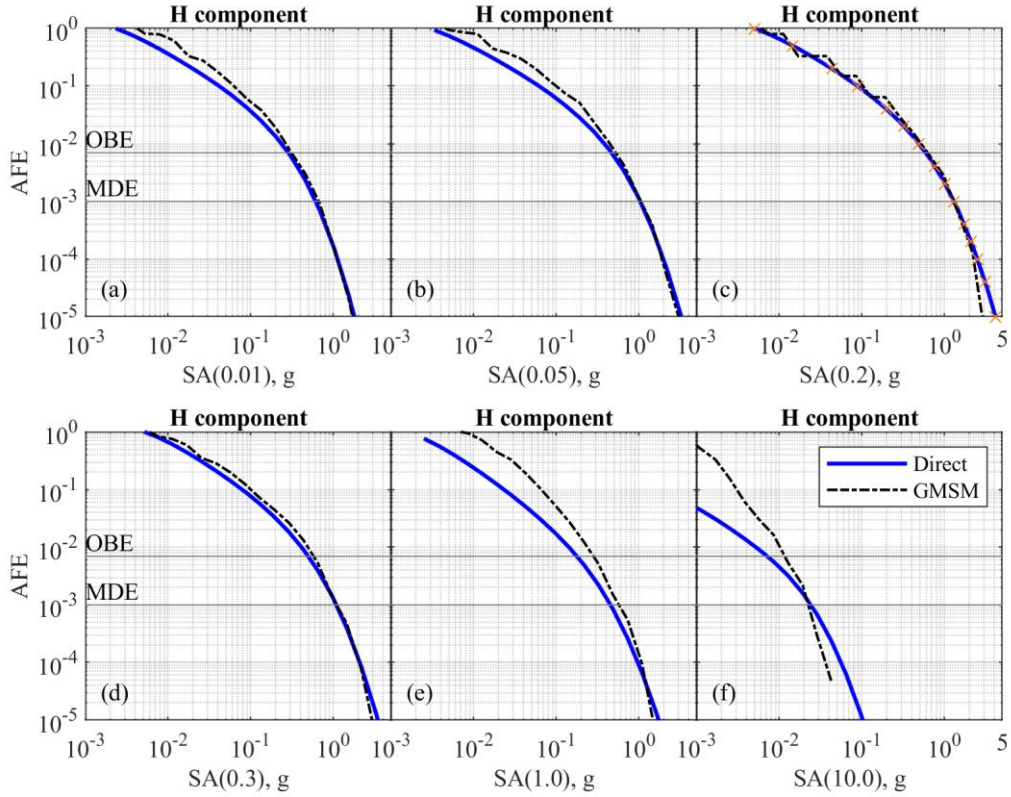

Figure 5. Hazard consistency evaluation via comparing ground motion model (GMM)-based versus ground motion selection and modification (GMSM)-based hazard curves for the horizontal (H) component of ground motion and spectral accelerations (SAs) at the following: (a) 0.01, (b) 0.05, (c) 0.2, (d) 0.3, (e) 1.0, and (f) 10.0 sec. The orange markers in panel (c) show the 15 return periods that were used to discretize Equation 7. AFE: annual frequency of exceedance; MDE: maximum design earthquake; OBE: operating basis earthquake.

As expected, the H hazard curves for $T = 0.2$ sec are in excellent agreement because the term $\widehat{\Pr}(SA_k(T) \geq y \mid SA_H(T^*) = x_i)$ in Equation 8 reduces to Heaviside step functions when $T = T^*$. For $T = 0.3$ sec, which represents lengthening of the fundamental period from slightly nonlinear seismic response, the H hazard curves are also in excellent agreement. For vibration periods farther away from T^*, the discrepancies between the H hazard curves increase. For $T = 0.05$ sec, which approximates $0.2T_1$ to represent higher-mode effects, the GMSM-based hazard curve overestimates the hazard at return periods shorter than the OBE but agrees with the GMM-based hazard curve at return periods longer than the OBE, which are commonly of interest in nonlinear RHA of concrete dams. For $T = 10$ sec, Figure 5f shows that the selected sets of multicomponent GMs are hazard *inconsistent* with respect to *SA*(10.0) along the H component of GM.

As indicated by Equation 8, a GMSM-based hazard curve is sensitive to many different user-specified inputs such as (i) number of return periods for discretizing the integral in Equation 7 (e.g., 3 versus 15 return periods), (ii) method of evaluating the integral in Equation 7 (e.g., summation versus trapezoidal rule), (iii) target spectra for selecting multicomponent GM time series to represent the probability distribution of $SA_k(T) \mid SA_H(T^*)$ (e.g., "Method 1" versus "Method 4" of CS per Lin et al. (2013a)), (iv) period range for comparing GM response spectra against corresponding target spectra (e.g., 0.01 sec to 10 sec versus $0.2T_1$ to $1.5T_1$ per Kwong and Chopra (2020)), and (v) degree of constraining scale factors (e.g., max scale factor of four versus unconstrained scale factors). Varying such inputs indicates that the main cause of hazard inconsistencies in Figure 5 arises from the use of "Method 1" CS herein instead of "Method 4" CS, which uses the full disaggregation output instead of a mean-based earthquake rupture scenario. Another potential cause of hazard inconsistencies is the lack of constraining GMs based on site class. The results in Figure 5 are consistent with the need to "inflate" the logarithmic standard deviation in the "Method 1" CS as described in Lin et al. (2013b).

How do the V components of the $n_{RP} = 15$ sets of multicomponent GMs compare against GMM-based hazard? Figure 6 answers this question. Specifically, the solid blue curves show the V hazard curves from substituting the BC2016V GMM for the V component of GM into Equation 1 (i.e., "direct" approach). By contrast, the dashed orange curves show the V hazard curves from first deriving the medians and logarithmic standard deviations for the V component via Equations 4 and 5 before applying Equation 1 (i.e., "indirect" approach). Because the CB2014, BC2016V, and BC2016V/H GMMs were confirmed to be internally consistent (Figure 3), it is expected that the V hazard curves from the "direct" and "indirect" approaches would be identical. However, if a different GMM for the V/H ratio was used for Equations 4 and 5 (e.g., the GMM by Gülerce and Abrahamson (2011)), differences in hazard would arise, which are important for quantifying epistemic uncertainties in hazard.

The chained black curves in Figure 6 show the V hazard curves from applying Equation 8 to spectral accelerations along the V component of GM from the $n_{RP} = 15$ sets of multicomponent GMs that condition upon $T^* = T_1 = 0.2$ sec (i.e., "GMSM" approach). Among the vibration periods shown, the selected GMs are most hazard consistent with respect to the V component of GM for periods of 0.2 sec and 0.3 sec. By contrast, the GMSM-based V hazard curve differs the most from the GMM-based V hazard curve at a vibration period of 10 sec (i.e., least hazard consistent). Without V hazard curves, it is impossible to evaluate hazard consistency of the selected sets of GMs with respect to the V component of GM before pursuing computationally intensive RHAs of concrete dams.

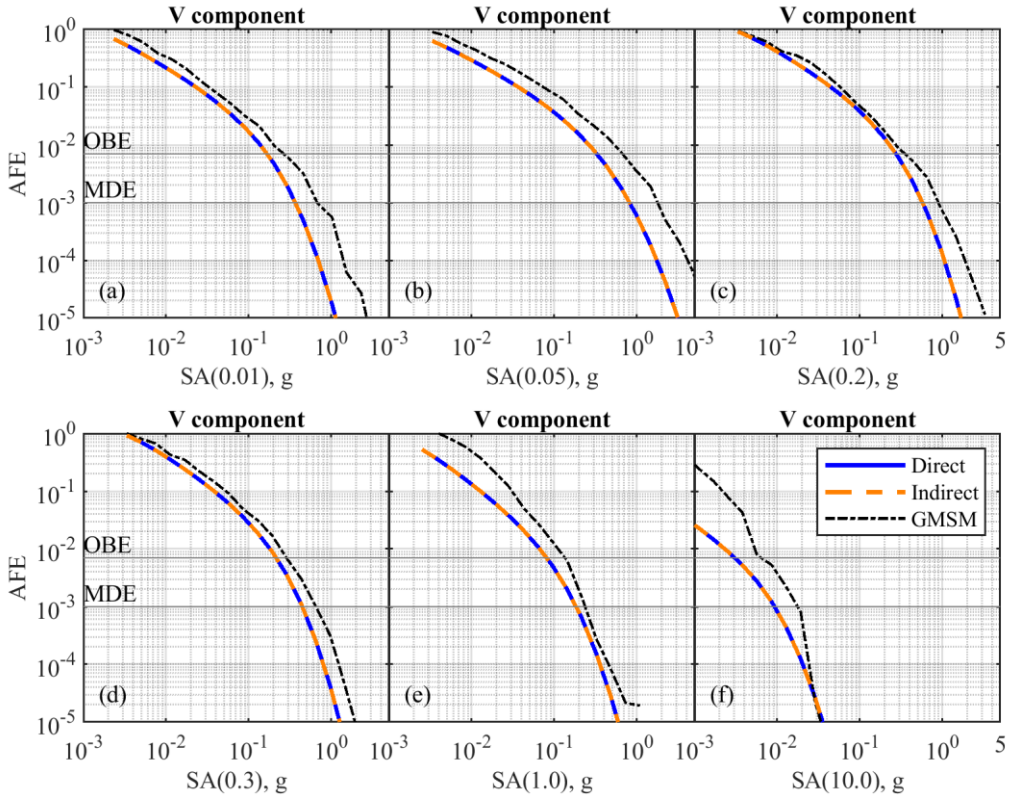

Figure 6. Hazard consistency evaluation via comparing ground motion model (GMM)-based versus ground motion selection and modification (GMSM)-based hazard curves for the vertical (V) component of ground motion and spectral accelerations (SAs) at the following: (a) 0.01, (b) 0.05, (c) 0.2, (d) 0.3, (e) 1.0, and (f) 10.0 sec. AFE: annual frequency of exceedance; MDE: maximum design earthquake; OBE: operating basis earthquake.

6. Limitations

To focus on the comparisons between different approaches to deriving V hazard, this study did not consider duration and near-source effects of GMs, which are also important to the seismic analysis of concrete dams. Further, limits to causal parameters such as magnitude and distance were not imposed in the GMSM process to avoid limiting the number of available GM time series; if such limits were desired without restricting the number of GMs, synthetic GMs could be used for selection instead of recorded GMs (e.g., Rezaeian and Der Kiureghian, 2010). Further, GMs were selected using the CS approach, whereas use of “exact” CS (i.e., Method 4 instead of Method 1) or the Generalized Conditional Intensity Measure methods would have resulted in improved hazard consistency for the H components of GM (Bradley, 2010; Lin et al., 2013a). Finally, the comparison of V hazard curves, particularly between indirect-based and GMSM-based, could be repeated for other tectonic regimes, sites, and GMMs even though GMMs for the V component of GM may not be available in such regimes.

7. Conclusions

V hazard curves are required for evaluating the quality of V components of selected GM time series that are used as inputs to nonlinear RHA of concrete dams. However, V hazard curves are rarely available. This study explored three alternative approaches for deriving V hazard curves, leading to the following conclusions:

1. If GMMs for the V component of GM are available for a given tectonic regime (e.g., active crustal), they can be substituted into customary PSHA calculations to derive V hazard curves (i.e., “direct” approach via Equation 1).
2. If GMMs for the V component of GM are unavailable for a given tectonic regime (e.g., subduction zone), a GMM for the V/H ratio could potentially be combined with GMMs for the H component of GM to derive V hazard curves (i.e., “indirect” approach via Equations 4 and 5).

3. Deriving V hazard curves from the "indirect" approach requires not only GMMs for the H component of GM and for V/H ratios, but also *correlation models* that estimate the correlation between the H component of GM and the V/H ratio, $\rho_{H,V/H}$.

4. The GMM for the H component of GM by Campbell & Bozorgnia 2014, the GMM for the V component of GM by Bozorgnia & Campbell (2016a), and the GMM for the V/H ratio by Bozorgnia & Campbell (2016b) were confirmed to be internally consistent with respect to deriving V hazard curves; a new equation was derived herein (Equation 6) to enable use of the between-event and within-event correlations from Bozorgnia & Campbell (2016b), $\rho_{H,V}^{(B)}$ and $\rho_{H,V}^{(W)}$, for estimating $\rho_{H,V/H}$.

5. Epistemic uncertainty in the V hazard can be captured partially through multiple GMMs for the H component of GM when combined with a GMM for the V/H ratio; however, it can be captured more fully by also considering multiple GMMs for the V/H ratio as well as multiple correlation models for estimating $\rho_{H,V/H}$.

6. If both the "direct" and "indirect" approaches cannot be used to derive V hazard curves for a given tectonic regime (e.g., it is deemed unacceptable to combine a GMM for the V/H ratio that was derived from active crustal data with GMMs for the H component of GM that were derived from subduction zone data), V hazard curves can be estimated from sets of multicomponent GM time series (i.e., "GMSM" approach via Equation 8). However, results from the GMSM approach are sensitive to many user-defined inputs such as (i) number of return periods for discretizing the integral in Equation 7, (ii) method of evaluating the integral in Equation 7, (iii) target spectra for selecting multicomponent GM time series to represent the probability distribution of $SA_V(T) \mid SA_H(T^*)$, (iv) number of records per return period, (v) size of candidate GM database, (vi) period range for comparing GM response spectra against corresponding target spectra, and (vii) degree of constraining scale factors (including the possibility of excessive downwards scaling).

8. Acknowledgments

The PEER Center is acknowledged for making it possible to download multicomponent GMs from the NGA-West2 online database. Review comments from Josh Corbett, Peter Powers, Brian Shiro, and Janet Carter have improved this manuscript and are greatly appreciated. Any use of trade, firm, or product names is for descriptive purposes only and does not imply endorsement by the U.S. Government.

9. References

Abrahamson, N.A., 2006. Seismic hazard assessment: problems with current practice and future developments, in: First European Conference on Earthquake Engineering and Seismology 2006 (1st ECEES). Presented at the First European conference on earthquake engineering and seismology, Swiss Society for Earthquake Engineering and Structural Dynamics, Geneva, Switzerland, pp. 8590–8606.

American Society of Structural Engineers (ASCE) Structural Engineering Institute, 2017. Minimum design loads and associated criteria for buildings and other structures (ASCE/SEI 7-16), American Society of Civil Engineers, Reston, VA, 822 pp. https://doi.org/10.1061/9780784414248

Ancheta, T.D., Darragh, R.B., Stewart, J.P., Seyhan, E., Silva, W.J., Chiou, B.S.-J., Wooddell, K.E., Graves, R.W., Kottke, A.R., Boore, D.M., others, 2014. NGA-West2 database. Earthquake Spectra 30, 989–1005. https://doi.org/10.1193/070913EQS197M

Applied Technology Council (ATC), 2012. Seismic Performance Assessment of Buildings; Volume 1- Methodology (FEMA P-58). Prepared for the Federal Emergency Management Agency, Redwood City, CA, 313 pp.

Basu, U., Chopra, A.K., 2004. Perfectly matched layers for transient elastodynamics of unbounded domains. International Journal for Numerical Methods in Engineering 59, 1039–1074. https://doi.org/10.1002/nme.896

Bazzurro, P., Cornell, C.A., 1999. Disaggregation of seismic hazard. Bulletin of the Seismological Society of America 89, 501–520. https://doi.org/10.1785/0120060093

Bernier, C., Monteiro, R., Paultre, P., 2016. Using the Conditional Spectrum method for improved fragility assessment of concrete gravity dams in eastern Canada. Earthquake Spectra 32, 1449–1468. https://doi.org/10.1193/072015EQS116M

Bozorgnia, Y., Abrahamson, N.A., Atik, L.A., Ancheta, T.D., Atkinson, G.M., Baker, J.W., Baltay, A., Boore, D.M., Campbell, K.W., Chiou, B.S., and others, 2014. NGA-West2 research project. Earthquake Spectra 30, 973–987. https://doi.org/10.1193/072113EQS209M

Bozorgnia, Y., Campbell, K.W., 2004. The vertical-to-horizontal response spectral ratio and tentative procedures for developing simplified V/H and vertical design spectra. Journal of Earthquake Engineering 8, 175–207. https://doi.org/10.1080/13632460409350486

Bozorgnia, Y., Campbell, K.W., 2016a. Vertical ground motion model for PGA, PGV, and linear response spectra using the NGA-West2 database. Earthquake Spectra 32, 979–1004. https://doi.org/10.1193/072814EQS121M

Bozorgnia, Y., Campbell, K.W., 2016b. Ground motion model for the vertical-to-horizontal (V/H) ratios of PGA, PGV, and response spectra. Earthquake Spectra 32, 951–978. https://doi.org/10.1193/100614EQS151M

Bradley, B.A., 2010. A generalized conditional intensity measure approach and holistic ground-motion selection. Earthquake Engineering & Structural Dynamics 39, 1321–1342. https://doi.org/10.1002/eqe.995

Bradley, B.A., 2012. The seismic demand hazard and importance of the conditioning intensity measure. Earthquake Engineering & Structural Dynamics 41, 1417–1437. https://doi.org/10.1002/eqe.2221

Building Seismic Safety Council (BSSC), 2009. NEHRP Recommended Seismic Provisions for New Buildings and Other Structures (FEMA P-750). Prepared for the Federal Emergency Management Agency, Washington, D.C., 388 pp.

Campbell, K.W., Bozorgnia, Y., 2014. NGA-West2 ground motion model for the average horizontal components of PGA, PGV, and 5% damped linear acceleration response spectra. Earthquake Spectra 30, 1087–1115. https://doi.org/10.1193/062913EQS175M

Chopra, A.K., 2020. Earthquake Engineering for Concrete Dams: Analysis, Design, and Evaluation. John Wiley & Sons, 320 pp.

Federal Emergency Management Agency (FEMA), 2005. Federal guidelines for dam safety: Earthquake analyses and design of dams (FEMA P-65). Federal Emergency Management Agency, Washington, DC, 75 pp.

Field, E.H., Jordan, T.H., Cornell, C.A., 2003. OpenSHA: A developing community-modeling environment for seismic hazard analysis. Seismological Research Letters 74, 406–419. https://doi.org/10.1785/gssrl.74.4.406

Gülerce, Z., Abrahamson, N.A., 2011. Site-specific design spectra for vertical ground motion. Earthquake Spectra 27, 1023–1047. https://doi.org/10.1193/1.3651317

Gülerce, Z., Kamai, R., Abrahamson, N.A., Silva, W.J., 2017. Ground motion prediction equations for the vertical ground motion component based on the NGA-W2 database. Earthquake Spectra 33, 499–528. https://doi.org/10.1193/121814EQS213M

Hariri-Ardebili, M.A., 2018. Risk, Reliability, Resilience (R3) and beyond in dam engineering: A state-of-the-art review. International journal of disaster risk reduction 31, 806–831.

Hariri-Ardebili, M.A., Saouma, V.E., 2016. Collapse fragility curves for concrete dams: Comprehensive study. Journal of Structural Engineering 142, 4016075. https://doi.org/10.1061/(ASCE)ST.1943-541X.0001541

Heppermann, B., Luco, N., 2020. Exploring the Use of “M9” Ground Motion Simulation for Seismic Risk Assessment of Dams. Proceedings of the 17th World Conference on Earthquake Engineering, Sendai, Japan, paper 1D-0123, 12 pp.

Jalayer, F., 2003. Direct probabilistic seismic analysis: Implementing non-linear dynamic assessments. PhD dissertation, Stanford University, Palo Alto, CA, 243 pp.

Jayaram, N., Lin, T., Baker, J.W., 2011. A computationally efficient ground-motion selection algorithm for matching a target response spectrum mean and variance. Earthquake Spectra 27, 797–815. https://doi.org/10.1193/1.3608002

Kwong, N.S., Chopra, A.K., 2020. Selecting, scaling, and orienting three components of ground motions for intensity-based assessments at far-field sites. Earthquake Spectra 36, 1013–1037. https://doi.org/10.1177/8755293019899954

Kwong, N.S., Chopra, A.K., McGuire, R.K., 2015. A framework for the evaluation of ground motion selection and modification procedures. Earthquake Engineering & Structural Dynamics 44, 795–815. https://doi.org/10.1002/eqe.2502

Kwong, N.S., Jaiswal, K.S., Luco, N., Baker, J.W., 2020. Selecting three components of ground motions from Conditional Spectra for multiple stripe analyses, Proceedings of the 17th World Conference on Earthquake Engineering. Sendai, Japan, paper C002724, 12 pp.

Lin, T., Harmsen, S.C., Baker, J.W., Luco, N., 2013a. Conditional Spectrum computation incorporating multiple causal earthquakes and ground-motion prediction models. Bulletin of the Seismological Society of America 103, 1103–1116. https://doi.org/10.1785/0120110293

Lin, T., Haselton, C.B., Baker, J.W., 2013b. Conditional Spectrum-based ground motion selection. Part I: Hazard consistency for risk-based assessments. Earthquake Engineering & Structural Dynamics 42, 1847–1865. https://doi.org/10.1002/eqe.2301

Lin, T., Haselton, C.B., Baker, J.W., 2013c. Conditional Spectrum-based ground motion selection. Part II: Intensity-based assessments and evaluation of alternative target spectra. Earthquake Engineering & Structural Dynamics 42, 1867–1884. https://doi.org/10.1002/eqe.2303

Løkke, A., Chopra, A.K., 2019. Direct finite element method for nonlinear earthquake analysis of concrete dams: Simplification, modeling, and practical application. Earthquake Engineering & Structural Dynamics 48, 818–842. https://doi.org/10.1002/eqe.3150

National Earthquake Hazards Reduction Program (NEHRP) Consultants Joint Venture, 2011. Selecting and scaling earthquake ground motions for performing response-history analyses (NIST GCR 11-917-15). Prepared for the National Institute of Standards and Technology, Gaithersburg, MD, 256 pp.

Rezaeian, S., Der Kiureghian, A., 2010. Simulation of synthetic ground motions for specified earthquake and site characteristics. Earthquake Engineering & Structural Dynamics 39, 1155–1180. https://doi.org/10.1002/eqe.997

Rezaeian, S., Powers, P.M., Altekruse, J.M., Ahdi, S.K., Petersen, M.D., Shumway, A.M., Frankel, A.D., Wirth, E.A., Smith, J.A., Moschetti, M.P., Withers, K.B., in press. The 2023 U.S. National Seismic Hazard Model: Subduction Ground Motion Models. Earthquake Spectra (accepted).

Stewart, J.P., Boore, D.M., Seyhan, E., Atkinson, G.M., 2016. NGA-West2 equations for predicting vertical-component PGA, PGV, and 5%-damped PSA from shallow crustal earthquakes. Earthquake Spectra 32, 1005–1031. https://doi.org/10.1193/070113EQS184M

Tarbali, K., Bradley, B.A., 2016. The effect of causal parameter bounds in PSHA-based ground motion selection. Earthquake Engineering & Structural Dynamics 45, 1515–1535. https://doi.org/10.1002/eqe.2721

U.S. Army Corps of Engineers, 2016. Earthquake Design and Evaluation for Civil Works Projects (No. ER 1110-2-1806). Department of the army, Washington, DC, 28 pp.

Zimmerman, R.B., Baker, J.W., Hooper, J.D., Bono, S., Haselton, C.B., Engel, A., Hamburger, R.O., Celikbas, A., Jalalian, A., 2017. Response History Analysis for the Design of New Buildings in the NEHRP Provisions and ASCE/SEI 7 Standard: Part III-Example Applications Illustrating the Recommended Methodology. Earthquake Spectra 33, 419–447. https://doi.org/10.1193/061814EQS087M